

Intramitochondrial Zn²⁺ accumulation via the Ca²⁺ uniporter contributes to acute ischemic neurodegeneration

Q1 Yuliya V. Medvedeva¹, John H. Weiss*

Q5 Q4 Department of Neurology, University of California, Irvine, Irvine, CA 92697, USA
 5 Department of Anatomy and Neurobiology, University of California, Irvine, Irvine, CA 92697, USA

ARTICLE INFO

Article history:
 7 Received 9 January 2014
 8 Revised 2 April 2014
 9 Accepted 21 April 2014
 10 Available online xxxx

Keywords:
 12 Hippocampal slice
 13 Mitochondria
 14 Zinc
 15 Calcium
 16 Ischemia
 17 Ruthenium Red
 18 RU360
 19 Mitochondrial Ca²⁺ uniporter
 20 Reactive oxygen species
 21 ROS

ABSTRACT

Ca²⁺ and Zn²⁺ have both been implicated in the induction of acute ischemic neurodegeneration. We recently examined changes in intracellular Zn²⁺ and Ca²⁺ in CA1 pyramidal neurons subjected to oxygen glucose deprivation (OGD), and found that Zn²⁺ rises precede and contribute to the onset of terminal Ca²⁺ rises (“Ca²⁺ deregulation”), which are causatively linked to a lethal loss of membrane integrity. The present study seeks to examine the specific role of intramitochondrial Zn²⁺ accumulation in ischemic injury, using blockers of the mitochondrial Ca²⁺ uniporter (MCU), through which both Zn²⁺ and Ca²⁺ appear able to enter the mitochondrial matrix. In physiological extracellular Ca²⁺, treatment with the MCU blocker, Ruthenium Red (RR), accelerated the Ca²⁺ deregulation, most likely by disrupting mitochondrial Ca²⁺ buffering and thus accelerating the lethal cytosolic Ca²⁺ overload. However, when intracellular Ca²⁺ overload was slowed, either by adding blockers of major Ca²⁺ entry channels or by lowering the concentration of Ca²⁺ in the extracellular buffer, Ca²⁺ deregulation was delayed, and under these conditions either Zn²⁺ chelation or MCU blockade resulted in similar further delays of the Ca²⁺ deregulation. In parallel studies using the reactive oxygen species (ROS) indicator, hydroethidine, lowering Ca²⁺ surprisingly accelerated OGD induced ROS generation, and in these low Ca²⁺ conditions, either Zn²⁺ chelation or MCU block slowed the ROS generation. These studies suggest that, during acute ischemia, Zn²⁺ entry into mitochondria via the MCU induces mitochondrial dysfunction (including ROS generation) that occurs upstream of, and contributes to the terminal Ca²⁺ deregulation.

© 2014 Published by Elsevier Inc.

Introduction

Although relatively short periods of cerebral ischemia can result in irreversible neuronal damage, the factors underlying the high ischemic vulnerability of brain tissue are incompletely understood. A contributory factor is the rapid influx of Ca²⁺ ions resulting from uncontrolled release of the excitatory neurotransmitter, glutamate, leading to the occurrence of sharp Ca²⁺ rises (“Ca²⁺ deregulation”) indicative of cell death (Randall and Thayer, 1992; Rothman and Olney, 1986; Siesjo, 1988). However, accumulating evidence supports critical contributions of another divalent cation, Zn²⁺, which is present in the brain at high levels. It accumulates in hippocampal pyramidal neurons after ischemia or prolonged seizures, and has also been implicated in ischemic neurodegeneration (Calderone et al., 2004; Frederickson et al., 1989; Koh et al., 1996; Tonder et al., 1990; Yin et al., 2002). Furthermore, like Ca²⁺, exogenous Zn²⁺ can be sequestered by mitochondria and impair

their function (Dineley et al., 2003; Shuttleworth and Weiss, 2011; Weiss et al., 2000). In addition, recent studies in hippocampal slice models have found that extracellular and intracellular Zn²⁺ levels increase shortly after onset of oxygen glucose deprivation (OGD) (Carter et al., 2011; Medvedeva et al., 2009; Stork and Li, 2006; Wei et al., 2004), and other studies have provided evidence that Zn²⁺ contributes to mitochondrial dysfunction following in vivo ischemia (Bonanni et al., 2006; Calderone et al., 2004).

We have used acute hippocampal slice models to attempt to discriminate contributions of Zn²⁺ vs Ca²⁺ to acute OGD-induced degeneration of CA1 pyramidal neurons. In our prior work, we found Zn²⁺ rises to precede the sharp Ca²⁺ rises (termed “Ca²⁺ deregulations”; Fig. 1A). Additionally, it was apparent that the Ca²⁺ deregulation events were causatively linked to a terminal loss of membrane integrity, since loss of membrane integrity (as indicated by rapid loss of fluorescent dye from the cell) began promptly after the sharp Ca²⁺ rises, and was prevented if Ca²⁺ was removed from the media during OGD, occurring only after restoration of the Ca²⁺ (Medvedeva et al., 2009). If Zn²⁺ was chelated, the Ca²⁺ deregulation (indicative of cell death) was delayed, implicating a contribution of Zn²⁺ to the terminal sequence of events. Furthermore, our results suggested that the Zn²⁺ entered mitochondria and affected their function, but did not clearly determine whether the

* Corresponding author at: Department of Neurology, University of California, Irvine, Irvine, CA 92697-4299, USA. Fax: +1 949 824 1668.

E-mail addresses: yvmedved@uci.edu (Y.V. Medvedeva), jweiss@uci.edu (J.H. Weiss).

Available online on ScienceDirect (www.sciencedirect.com).

¹ Department of Neurology, University of California, Irvine, Irvine, CA 92697-4299, USA.

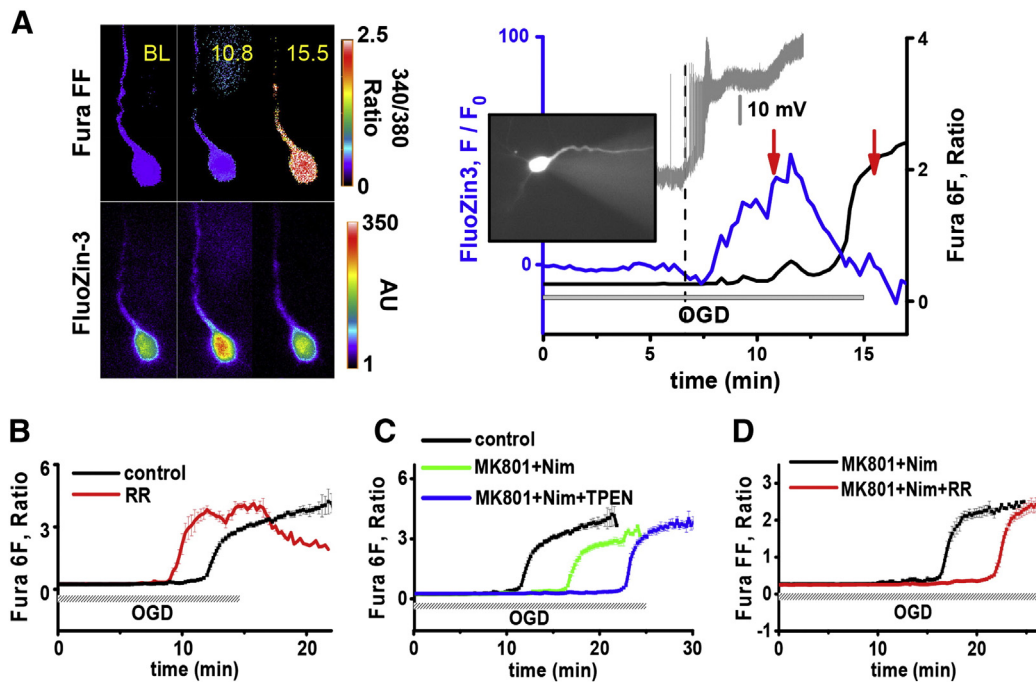


Fig. 1. Zn^{2+} and Ca^{2+} both contribute to OGD evoked neuronal injury. Individual CA1 neurons were co-loaded with low affinity ratiometric Ca^{2+} indicators Fura-FF (A,D) or Fura-6F (B,C) and the Zn^{2+} sensitive indicator FluoZin-3, and the slices were subjected to OGD. A: Relationship between plasma membrane depolarization and intracellular Zn^{2+} and Ca^{2+} rises in an individual CA1 neuron subjected to OGD. Left: Pseudocolor fluorescent images of a CA1 neuron co-loaded with Fura-FF (top, 340/380 ratio images) and FluoZin-3 (bottom, background subtracted emission intensity, arbitrary units) and subjected to 15 min OGD. Numbers indicate time (in min) following the onset of OGD (BL = base line). Right: Traces show changes in membrane potential (gray), FluoZin-3 fluorescence (blue) and Fura-FF ratio (black) in the CA1 neuron. Inset shows fluorescent image (Ex: 380 nm) to display the cytosolic distribution of the Fura-FF (the gray triangle to the right is an artifact of the attached patch pipette). Arrows indicate time points (10.8 and 15.5 min) of the images shown (Left). Note that the membrane depolarization (occurring after 6.7 ± 0.3 min, $n = 3$) begins shortly before the Zn^{2+} rise, and that the Zn^{2+} rise precedes the Ca^{2+} deregulation. B–D: All traces depict mean Fura-6F 340/380 ratio changes (\pm SEM), and, for clarity of display, are aligned for the onset of Ca^{2+} deregulation. OGD bars show approximate start and end time of the OGD episode, reflecting mild variations in the precise Ca^{2+} deregulation times in different slices. B: In physiological (2 mM) $[Ca^{2+}]_e$, the mitochondrial Ca^{2+} uniporter (MCU) blocker, Ruthenium Red (RR) accelerates OGD evoked Ca^{2+} deregulation. Slices were subjected to OGD alone or with RR (10 μ M, 15 min prior to and during the 15 min OGD episode). (Ca^{2+} deregulation occurred after 11.5 ± 0.4 min in control, black, $n = 10$; vs 8.7 ± 0.53 min with RR, red, $n = 10$; $p < 0.005$). C: Ca^{2+} entry blockers and Zn^{2+} chelation additively delay OGD evoked Ca^{2+} deregulation. Combined application of the NMDA receptor blocker MK-801 (10 μ M) and the VGCC blocker nimodipine (10 μ M) delays Ca^{2+} deregulation (from 11.5 ± 0.4 , $n = 10$, black, in control to 16.4 ± 1.0 , $n = 9$, green, with blockers, $p < 0.005$), and Ca^{2+} deregulation is further delayed by addition of the Zn^{2+} chelator TPEN (to 22.7 ± 1.5 , $n = 8$, blue, $p < 0.005$ vs blockers alone). All drugs were applied 10 min prior to and during the OGD episode. D: In the presence of MK-801 and nimodipine, RR delays Ca^{2+} deregulation (from 16.3 ± 1.34 min, $n = 7$, black, in the presence of blockers alone to 21.9 ± 1.61 min, $n = 9$, red, with blockers and RR, $p < 0.05$). RR was applied 15 min prior to and during 25 min OGD episode.

Zn^{2+} effects were dependent upon the mitochondrial Zn^{2+} entry (Medvedeva et al., 2009).

A central aim of the present study was thus to further examine the specific mechanisms through which Zn^{2+} contributes to the sequence of events during acute OGD that culminates in the terminal Ca^{2+} deregulation, specifically addressing the question of the dependence of its effects upon uptake into mitochondria. Our findings support the hypothesis that early Zn^{2+} entry into mitochondria through the mitochondrial Ca^{2+} uniporter (MCU) contributes to mitochondrial dysfunction and reactive oxygen species (ROS) production occurring upstream from the Ca^{2+} deregulation, highlighting these events as potential targets for therapeutic intervention in ischemia.

Materials and methods

Animals

Animal procedures were conducted in accordance with protocols approved by the Institutional Animal Care and Use Committee of the University of California at Irvine. Efforts were made to minimize animal suffering and number of mice used.

Preparation of acute hippocampal slices

Hippocampal slices (300 μ m) were prepared from 4 week old 129S6/SvEvTac mice (Taconic Farms, Inc.) as previously described (Medvedeva et al., 2009). Briefly slices were cut with a vibratome

(VT-1200, Leica Microsystems, Germany) in chilled cutting solution, 103 containing (in mM): KCl 3, NaH_2PO_4 1.25, $CaCl_2$ 0.2, $MgSO_4$ 6, $NaHCO_3$ 104 26, sucrose 220, glucose 10 and ketamine 0.43 (pH 7.35, 310 mOsm, 105 equilibrated with 95% O_2 /5% CO_2) and transferred into artificial cerebrospinal fluid (ACSF) containing (in mM): NaCl 126, KCl 3, NaH_2PO_4 1.25, 106 $CaCl_2$ 2, $MgSO_4$ 1, $NaHCO_3$ 26, and glucose 10 (pH 7.35, adjusted with 107 sucrose to 310 mOsm and equilibrated with 95% O_2 /5% CO_2) and incubated for 1 h at 34 $^\circ$ C. 108 109

OGD exposures and low $[Ca^{2+}]_e$ experiments

To simulate hypoxic–hypoglycemic conditions, ACSF was replaced 112 with identical solution but lacking glucose (glucose was substituted 113 with an equimolar concentration of sucrose) and equilibrated with 114 95% N_2 /5% CO_2 . For low $[Ca^{2+}]_e$ experiments, we prepared ACSF in 115 which 1.8 mM Ca^{2+} was substituted with Mg^{2+} (thus containing 116 200 μ M of Ca^{2+} and 2.8 mM of Mg^{2+}). 117

Loading individual hippocampal CA1 neurons with Ca^{2+} and Zn^{2+} sensitive fluorescent indicators and fluorescence measurements

For recordings slices were placed in a flow-through chamber (RC- 120 27L, Warner Instruments; Hamden, CT) mounted on the stage of an 121 upright microscope (BX51WI, Olympus, Japan) and superfused with 122 oxygenated ACSF (95% O_2 /5% CO_2) at 2 ml/min. Experiments were 123 performed at 32 ± 0.5 $^\circ$ C. 124

125 For simultaneous measurements of intracellular Ca^{2+} ($[\text{Ca}^{2+}]_i$)
 126 and Zn^{2+} ($[\text{Zn}^{2+}]_i$) dynamics, cells were co-loaded with the low af-
 127 finity Ca^{2+} sensitive indicator Fura-6F ($K_{d\text{Ca}} \sim 5.3 \mu\text{M}$) or Fura-FF
 128 ($K_{d\text{Ca}} \sim 5.5 \mu\text{M}$), and the high affinity Zn^{2+} sensitive indicator
 129 FluoZin-3 ($K_d \sim 15 \text{nM}$) via patch pipettes as described previously
 130 **Q6** (12). Fluorescent indicators were dissolved in pipette solution (contain-
 131 ing (mM): 125 K Gluconate, 10 KCl, 3 Mg-ATP, 1 MgCl_2 , 10 HEPES,
 132 pH 7.25 with KOH (290 mOsm with sucrose) to 1 mM, and a 1 μl droplet
 133 **Q7** placed in pipette).

134 Fluorescence was alternately excited at 340, 380 for Fura-6F or Fura-
 135 FF and 482 nm for FluoZin-3 (using 20 nm bandpass filters, Semrock Inc.,
 136 USA) via a $40\times$ water-immersion objective (numerical aperture 0.8,
 137 Olympus) and emission for both indicators collected at 532(40) nm
 138 using a CCD camera (Hamamatsu, Japan). Images were acquired at 15 s
 139 intervals and analyzed, after background subtraction, with METAFLUOR
 140 7.1.7 software (Molecular Devices, Union City, CA). Changes in $[\text{Ca}^{2+}]_i$
 141 are presented as the ratio of background subtracted emission intensities
 142 upon excitation at 340 and 380 nm (“340/380 ratio”), and $[\text{Zn}^{2+}]_i$
 143 changes are presented as $\Delta F/F_0 = (F_x - F_0) / F_0$, where F_x is the back-
 144 ground subtracted fluorescence at each time point, x , and F_0 is the aver-
 145 age background subtracted baseline fluorescence over the 10 min prior
 146 to OGD. The onset times of OGD-induced Zn^{2+} rises and of Ca^{2+} dereg-
 147 ulations were determined by finding intersections between the extrapolat-
 148 ed baselines, with lines fitting the first substantial FluoZin-3 fluorescence
 149 increases or Fura-6F ratio increases, as previously described (Medvedeva
 150 et al., 2009). To track membrane potential changes during OGD, the patch
 151 electrode was left attached to the CA1 neuron, and the potential was
 152 monitored in whole cell current clamp configuration.

153 *Measuring increase in reactive oxygen species (ROS) production evoked by* 154 *OGD*

155 To access changes in ROS production in response to OGD, we used
 156 the superoxide preferring ROS indicator, hydroethidine (HET), which is
 157 oxidized into the highly fluorescent compound, ethidium. Slices were
 158 bath loaded with HET (20 μM , 30 min at 22–25 °C), subjected to OGD,
 159 and regions of interest were monitored in the CA1 pyramidal cell
 160 layer. HET was excited at 540(25) nm and emitted fluorescence was col-
 161 lected at 605(55) nm. For simultaneously HET and Fura-6F imaging, HET
 162 was excited at 482(20) nm and emission collected at 532(40) nm,
 163 resulting in some decrement in the fluorescence signal. Data are pre-
 164 sented as $\Delta F/F_0 = (F_x - F_0) / F_0$, where F_x is the fluorescence at each
 165 time point, x , and F_0 is the baseline fluorescence, averaged over 5 min
 166 before OGD.

167 To quantify and compare ROS production across slices, the near lin-
 168 ear sharply rising phase of each HET ΔF trace (typically starting ~5–
 169 8 min and extending for 2–5 more min) was linearly fitted (to elicit a
 170 slope standard error, SE, <0.1 ; see Fig. 3A), and the slope, m , of this
 171 phase compiled across matched sets of control and treatment slices. Of
 172 note, whereas Ca^{2+} deregulation times were quite closely reproducible
 173 across experimental animals and slice preparations, absolute HET ΔF rise
 174 slopes were highly variable across slice sets, and for this reason all com-
 175 parisons were made on matched sets of slices, with near equal (± 1)
 176 numbers of control and treatment slices obtained from each prepara-
 177 tion. Each set of slices was obtained from at least 3 animals.

178 *Reagents*

179 Fura-6F, Fura-FF, FluoZin-3 and hydroethidine (dihydroethidium)
 180 were obtained from Invitrogen (Carlsbad, CA). RU360 was purchased
 181 from Calbiochem (EMD Biosciences, La Jolla, CA), MK-801, Ruthenium
 182 Red, and N,N,N',N'-Tetrakis(2-pyridylmethyl)ethylenediamine (TPEN)
 183 were obtained from Sigma (St. Louis, MO). Nimodipine was obtained
 184 from Miles Inc. (West Haven, CT). All other reagents were purchased
 185 from Fisher Scientific.

Statistics

Data were analyzed using Origin 9.0 software. All differences be-
 187 tween control and treatment groups were assessed by 2-tailed t tests. 188

Results

In physiological Ca^{2+} , MCU blockade accelerates Ca^{2+} deregulation and cell death

To examine Ca^{2+} and Zn^{2+} changes in hippocampal CA1 pyramidal
 192 neurons during OGD, single neurons in acute slices were co-loaded with
 193 membrane impermeable forms of the high affinity Zn^{2+} indicator
 194 FluoZin-3 ($K_d \sim 15 \text{nM}$) and a low affinity Ca^{2+} indicator (Fura-6F, K_d
 195 $\sim 5.3 \mu\text{M}$; or Fura-FF, $K_d \sim 5.5 \mu\text{M}$) via a patch pipette (see Materials
 196 and methods section). In our prior work, we found OGD evoked Zn^{2+}
 197 rises to precede the sharp Ca^{2+} rises (termed “ Ca^{2+} deregulations”).
 198 In addition, as discussed in the introduction, it was apparent that the
 199 Ca^{2+} deregulation events were causatively linked to a terminal loss of
 200 membrane integrity. If Zn^{2+} was chelated, the lethal Ca^{2+} deregulation
 201 was delayed, and there was enhanced recovery of mitochondrial func-
 202 tion, implicating a contribution of Zn^{2+} , likely in part via effects on mi-
 203 tochondria, to the terminal injury cascade (Medvedeva et al., 2009). 204

As neuronal depolarization is a well described early event in ische-
 205 mic injury cascades, in order to better characterize our model, we
 206 sought to determine the relationship between the depolarization and
 207 the above described Zn^{2+} and Ca^{2+} rises. To do so, after indicator load-
 208 ing, we left the CA1 neuron in whole cell current clamp configuration to
 209 monitor membrane potential changes during OGD. In line with prior
 210 studies of depolarization of hippocampal neurons in slice during OGD
 211 (Yamamoto et al., 1997), we found depolarization to begin after
 212 ~6–7 min, shortly before the start of the cytosolic Zn^{2+} rise, and well be-
 213 fore the terminal Ca^{2+} deregulation (Fig. 1A). 214

The present study seeks to examine the specific contributions of
 215 Ca^{2+} and Zn^{2+} entry into mitochondria to the sequence of events lead-
 216 ing to neurodegeneration during acute OGD. As the mitochondrial Ca^{2+}
 217 uniporter (MCU) provides the primary route for Ca^{2+} passage across
 218 the inner mitochondrial membrane into the matrix (Bernardi, 1999;
 219 Kirichok et al., 2004), and appears to permit Zn^{2+} entry as well
 220 (Gazaryan et al., 2007; Jiang et al., 2001; Malaiyandi et al., 2005; Saris
 221 and Niva, 1994), we next examined effects of MCU blockade. When
 222 10 μM of the MCU blocker, Ruthenium Red (RR) (Moore, 1971) was
 223 added to the extracellular buffer prior to and during a 15 min OGD epi-
 224 sode, the Ca^{2+} deregulation was accelerated (occurring after $8.7 \pm$
 225 0.53 min vs $11.5 \pm 0.4 \text{ min}$ in control; Fig. 1B). Since mitochondria are im-
 226 portant high capacity buffers of intracellular Ca^{2+} loads, we considered
 227 whether block of mitochondrial Ca^{2+} uptake by RR might directly facili-
 228 tate the occurrence of the lethal cytosolic Ca^{2+} deregulation, thus ob-
 229 scuring the ability to resolve effects of mitochondrial Zn^{2+} uptake. For
 230 this reason, we examined the effect of adding blockers of two major
 231 routes of Ca^{2+} entry: N-methyl-D-aspartate (NMDA) channels and volt-
 232 age gated Ca^{2+} channels (VGCCs). Since we expected that the presence
 233 **Q8** of these channel blockers would delay the onset of Ca^{2+} deregulation, in
 234 these experiments, the OGD duration was increased to 25 min. Addition
 235 of the NMDA channel blocker MK-801 (10 μM) and the VGCC blocker
 236 nimodipine (10 μM) during OGD modestly delayed the time of the
 237 Ca^{2+} deregulation (to $16.4 \pm 1.0 \text{ min}$ from $11.5 \pm 0.4 \text{ min}$ in control;
 238 Fig. 1C). Moreover, similar to the results obtained in the absence of
 239 the Ca^{2+} entry blockers (Medvedeva et al., 2009), Zn^{2+} chelation with
 240 the high affinity membrane permeable Zn^{2+} chelator TPEN (40 μM) fur-
 241 ther delayed the Ca^{2+} deregulation (to $22.7 \pm 1.5 \text{ min}$; Fig. 1C). And fi-
 242 nally, when cytosolic Ca^{2+} loading was decreased by the Ca^{2+} entry
 243 blockers, further MCU inhibition with RR had the opposite effect as
 244 seen without blockers, significantly delaying the Ca^{2+} deregulation to
 245 a similar degree as Zn^{2+} chelation with TPEN (to $21.9 \pm 1.61 \text{ min}$;
 246 Fig. 1D), consistent with our hypothesis that rapid cytoplasmic Ca^{2+}
 247

248 accumulation in the presence of RR precluded the ability to resolve possible
249 beneficial effects of MCU blockade, such as inhibition of mitochondrial
250 Zn^{2+} uptake.

251 Thus, to simplify the paradigm and avoid possible complications due
252 to variable tissue penetrance or non-specific effects of the Ca^{2+} entry
253 blockers, we next carried out experiments in which, instead of adding
254 MK-801 and nimodipine, slices were bathed in artificial cerebrospinal
255 fluid (ACSF) buffer in which the Ca^{2+} concentration ($[Ca^{2+}]_e$) was
256 lowered from a physiological level (2 mM) to 200 μM . Under these con-
257 ditions, Ca^{2+} deregulation was substantially delayed (to $19.4 \pm$
258 1.26 min; Fig. 2A). Similar to the results observed in 2 mM $[Ca^{2+}]_e$ in
259 the absence (Medvedeva et al., 2009) or presence (Fig. 1C) of Ca^{2+}
260 channel blockers, Zn^{2+} chelation with TPEN resulted in a significant fur-
261 ther delay of the Ca^{2+} deregulation (to 27.4 ± 0.47 min; Fig. 2A), indi-
262 cating that in low $[Ca^{2+}]_e$, Zn^{2+} still significantly contributes to the
263 neurodegenerative cascade.

264 Furthermore, with 200 μM $[Ca^{2+}]_e$, MCU blockade with RR had a
265 similar effect to that seen in 2 mM $[Ca^{2+}]_e$ with Ca^{2+} entry blockers,
266 markedly delaying the Ca^{2+} deregulation (to 34.1 ± 1.81 min; Figs.
267 2B,E). Since, in these experiments, Ca^{2+} deregulation occurred well
268 after the end of the 25 min OGD episode, we carried out a set of exper-
269 iments in which OGD was extended beyond the onset of Ca^{2+} deregula-
270 tion (“continuous OGD”), and, as expected, MCU inhibition still
271 substantially delayed the Ca^{2+} deregulation (to $28.9.1 \pm 2.1$ min; see
272 supplemental Fig. S1). Although RR is a widely used MCU blocker, it is
273 not completely selective, also having effects on other cellular channels
274 (Tapia and Velasco, 1997). Therefore, to further confirm the neuropro-
275 tective effects of MCU inhibition against OGD induced neuronal injury
276 in low $[Ca^{2+}]_e$ conditions, experiments were repeated using the more
277 selective RR derivative, RU360 (Matlib et al., 1998). For these studies,
278 as RU360 is highly oxidation sensitive and unstable in solution, rather
279 than bath loading the slice, RU360 was mixed with deoxygenated intra-
280 cellular solution just prior to use, and introduced directly into the select-
281 ed CA1 pyramidal neuron via the patch electrode along with fluorescent
282 indicators. RU360 had similar protective effect as observed with bath

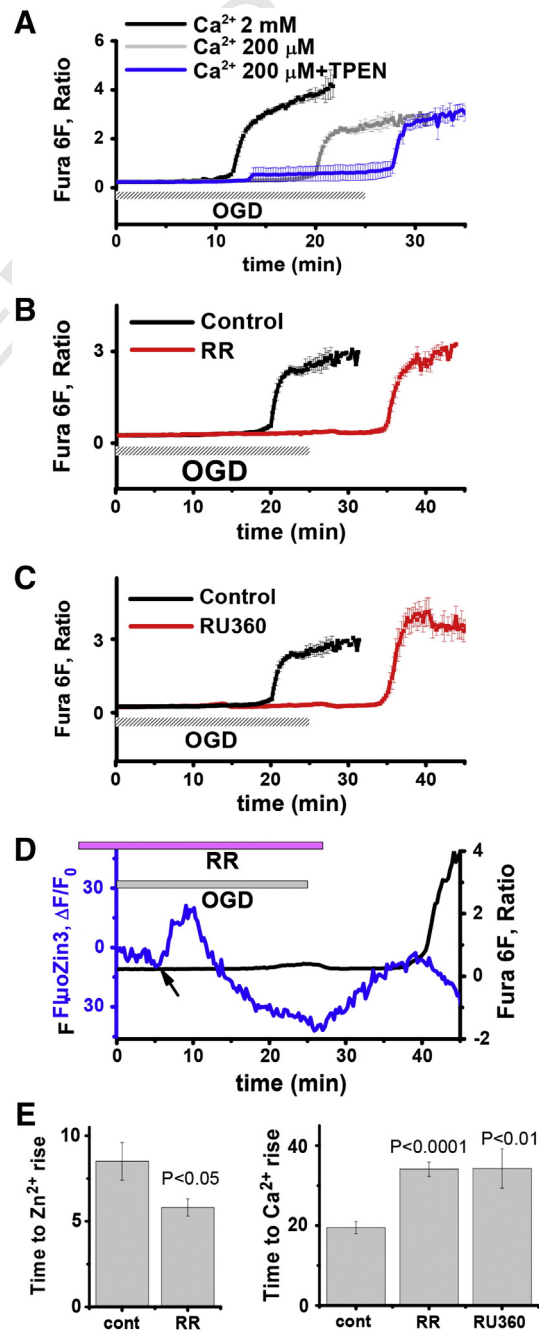
application of RR (delaying Ca^{2+} deregulation to 34.25 ± 4.9 min; 283
Figs. 2C,E). 284

285 We wondered whether the protective effects of MCU blockers
286 against OGD induced Ca^{2+} deregulation in low $[Ca^{2+}]_e$ might be due
287 to blockade of Zn^{2+} entry into mitochondria. Consistent with this
288 idea, the presence of RR during OGD in low $[Ca^{2+}]_e$ ACSF not only
289 reproduced (and modestly exceeded) the protective effect of TPEN,
290 but also accelerated the onset of cytosolic Zn^{2+} rises (to 5.8 ± 0.5 min
291 vs 8.3 ± 0.9 min in control; Figs. 2D,E).

Zn^{2+} contributes to OGD induced ROS generation 292

293 Despite strong evidence that ROS generation contributes to ischemic
294 neuronal injury (Chan, 2001; Kuroda and Siesjo, 1997), dynamics of
295 ischemia-associated ROS generation have been little studied. Thus, in
296 subsequent studies we utilized the superoxide preferring ROS indicator, 296

Fig. 2. In low $[Ca^{2+}]_e$, either Zn^{2+} chelation or MCU inhibition delays OGD evoked Ca^{2+} deregulation. Individual CA1 neurons were loaded with Fura-6F and FluoZin-3 as described and subjected to a 25 min episode of OGD in 200 μM $[Ca^{2+}]_e$. A: Decreasing $[Ca^{2+}]_e$ to 200 μM and Zn^{2+} chelation additively delay OGD evoked Ca^{2+} deregulation. Slices were subjected to OGD in 2 mM $[Ca^{2+}]_e$ (black), or in 200 μM $[Ca^{2+}]_e$ either alone (gray) or with the additional presence of TPEN (40 μM , 10 min before and during the OGD episode, blue) (Ca^{2+} deregulation occurred after 11.5 ± 0.4 min in 2 mM $[Ca^{2+}]_e$, $n = 10$; vs 19.4 ± 1.26 min in 200 μM $[Ca^{2+}]_e$, $n = 7$, $p < 0.0001$ and after 27.4 ± 0.47 min with TPEN in 200 μM $[Ca^{2+}]_e$, $n = 6$, $p < 0.002$, compared to low Ca^{2+} alone). B: In low (in 200 μM) $[Ca^{2+}]_e$, RR delays OGD evoked Ca^{2+} deregulation. Slices were subjected to OGD alone or with RR (10 μM , 15 min prior, during and for 5 min after the OGD episode). Traces depict mean Fura-6F ratio changes (\pm SEM), and, as above, are aligned for onset of Ca^{2+} deregulation (occurring after 19.4 ± 1.26 min in control, black, $n = 7$; vs 34.1 ± 1.81 min with RR, red, $n = 6$, $p < 0.0001$). C: In low (in 200 μM) $[Ca^{2+}]_e$, the selective MCU inhibitor, RU360 delays OGD evoked Ca^{2+} deregulation. RU360 was pipette loaded into individual CA1 neurons (along with Fura-6F and FluoZin-3). Traces depict mean Fura-6F ratio changes (\pm SEM), and, as above, are aligned for onset of Ca^{2+} deregulation (occurring after 19.4 ± 1.26 min in control, black, $n = 7$; vs 34.25 ± 4.9 min, red, $n = 4$, $p < 0.01$). D: RR exposure during OGD results in an accelerated intracellular Zn^{2+} rise. Traces depict FluoZin-3 ($\Delta F/F_0$, blue) and Fura-6F ratio (black) changes in a single representative CA1 pyramidal neuron subjected to OGD in low $[Ca^{2+}]_e$ and the presence of RR. The arrow denotes the onset of the Zn^{2+} rise. (The Zn^{2+} rise occurred at 8.3 ± 0.9 min, $n = 7$ in control; vs 5.8 ± 0.5 min, $n = 5$ with RR, $p < 0.05$, see E, below). After the sharp Zn^{2+} rise, the progressive decrease in FluoZin-3 fluorescence is due to neuronal swelling that accompanies the ischemic insult, reflecting dilution of the indicator. The subsequent rise in $\Delta F/F_0$, at the time of RR washout reflects the fact that RR has a partial quenching effect on FluoZin-3 fluorescence, and the late decrease in fluorescence occurring at the time of Ca^{2+} deregulation reflects a combination of highly accelerated swelling and loss of membrane integrity of the terminally injured cell, resulting in rapid dilution and loss of indicator. Notably, all of these effects seen with single wavelength indicators like FluoZin-3 are not seen with ratiometric indicators like Fura 6F, where the trace displays the ratio of emissions upon excitation at 340 and 380 nm that is substantially independent of dilution. E: Effects of MCU blockers on the time of the Zn^{2+} rise (left) and the time of the Ca^{2+} deregulation (right). Bars depict mean values in minutes (\pm SEM).



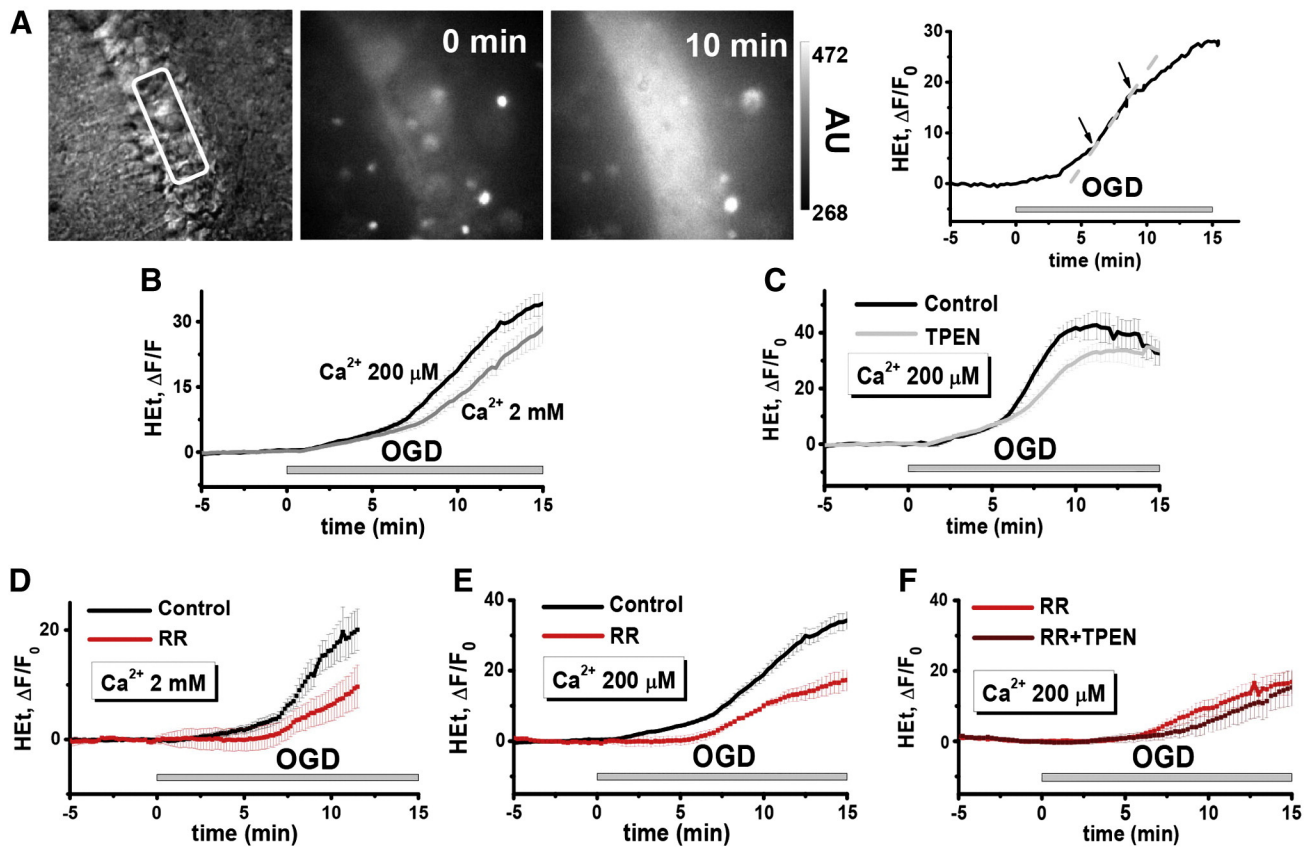


Fig. 3. OGD evokes ROS generation in CA1 pyramidal neurons. Slices were bulk loaded with the superoxide preferring ROS indicator, hydroethidine (HET, 20 μM for 30 min) and subjected to 15 min OGD. **A:** OGD evokes HET fluorescence increases (HET ΔF) in CA1 neurons. A differential interference contrast image (left) shows the CA1 pyramidal cell layer from which HET fluorescence changes were recorded; fluorescence images (middle, right) show representative HET fluorescence before and after 10 min OGD as indicated. Trace (far right) shows HET fluorescence changes (as $\Delta\text{F}/\text{F}_0$) in this slice in the region indicated by the rectangle. Arrows show approximate time of the steep phase of the HET ΔF rise, used for linear fitting for slope determination (as described in the **Materials and methods** section); the dashed line shows a linear fit of this region. **B:** Decreasing $[\text{Ca}^{2+}]_e$ accelerates OGD evoked ROS production. A set of matched slices was subjected to OGD. Graph represents mean HET ΔF ($\pm\text{SEM}$) in the CA1 region of the hippocampus in slices subjected to OGD in 2 mM (gray, $n = 12$ slices) or 200 μM $[\text{Ca}^{2+}]_e$ (black, $n = 13$ slices). Slopes of the steep phases of the HET ΔF rises were determined by linear fitting as described (see **Materials and methods** section; also A, above); based on this analysis, we found the mean slope (m) of the HET ΔF to be increased in low $[\text{Ca}^{2+}]_e$ (from $m = 3.22 \pm 0.34$ in 2 mM $[\text{Ca}^{2+}]_e$, gray, $n = 12$; to 4.26 ± 0.35 , black, $n = 13$ slices, in 200 μM $[\text{Ca}^{2+}]_e$; $p < 0.05$). **C:** Zn^{2+} chelation slows ROS production during OGD carried out in low $[\text{Ca}^{2+}]_e$. Slices were subjected to OGD in 200 μM $[\text{Ca}^{2+}]_e$ alone, or with TPEN. The presence of TPEN significantly slowed the HET ΔF rise (from $m = 9.82 \pm 0.82$ in control, black, $n = 7$; to 6.42 ± 0.41 with TPEN, gray, $n = 8$ slices, $p < 0.005$). **D:** In 2 mM $[\text{Ca}^{2+}]_e$, MCU inhibition slows HET ΔF increase during OGD. Brain slices were subjected to OGD along (black, $n = 5$ slices) or in the presence of RR (10 μM , 15 min before and during OGD, red, $n = 5$ slices). Traces show mean OGD evoked HET ΔF ($\pm\text{SEM}$) in the CA1 region. However, in this condition, the accelerated neuronal death with RR causes loss of indicator and prevents accurate quantification of the HET ΔF slopes. **E:** In low $[\text{Ca}^{2+}]_e$, OGD evoked ROS production is attenuated by MCU inhibition. Slices were subjected to OGD in 200 μM $[\text{Ca}^{2+}]_e$ alone, or with RR. The presence of RR markedly slowed the HET ΔF rise (from $m = 4.1 \pm 0.5$, black, $n = 8$ in control to 1.96 ± 0.33 , red, $n = 6$ slices with RR, $p < 0.02$). Traces show mean OGD evoked HET ΔF ($\pm\text{SEM}$) in the CA1 region. **F:** Combined Zn^{2+} chelation and MCU inhibition has no greater effect on ROS production during OGD, than MCU inhibition alone. Slices were subjected to OGD in 200 μM $[\text{Ca}^{2+}]_e$ with RR (red, $m = 1.96 \pm 0.33$, $n = 6$ slices) or with both RR and TPEN (brown, $m = 2.12 \pm 0.24$, $n = 5$ slices, $p > 0.05$).

325 hydroethidine (HET) (Bindokas et al., 1996; Carriedo et al., 1998) to
 326 examine contributions of Ca^{2+} and Zn^{2+} to OGD induced ROS generation.
 327 In the presence of ROS, HET is oxidized into highly fluorescent ethidium;
 328 the rate of HET fluorescence increase (HET ΔF) provides a measure of the
 329 ROS generation rate. After bath loading with HET, slices were placed in
 330 the recording chamber and subjected to OGD (15 min). A slow acceleration
 331 of HET ΔF typically occurred after ~1–3 min with a marked accelera-
 332 tion in ΔF occurring slightly later (typically between 5 and 9 min); a
 333 steep linear ΔF rise typically lasted for 2–5 more minutes (Fig. 3), before
 334 slowing due to pronounced cellular swelling. To quantify and compare
 335 rates of HET ΔF rise, slopes (m) of these steep phases in the HET ΔF
 336 rise were obtained through linear fitting (see **Materials and methods**
 337 section; Fig. 3A). In both high and low $[\text{Ca}^{2+}]_e$, the HET ΔF rise preceded
 338 the Ca^{2+} deregulation (supplemental Fig. S2). Despite the marked delay
 339 in the time of Ca^{2+} deregulation, when $[\text{Ca}^{2+}]_e$ was lowered to 200 μM ,
 340 the HET ΔF was distinctly altered, rising more sharply compared to that
 341 in the presence of 2 mM Ca^{2+} (to $m = 4.26 \pm 0.35$ vs 3.22 ± 0.34 in
 342 2 mM $[\text{Ca}^{2+}]_e$; Fig. 3B). To examine possible contributions of Zn^{2+} to
 343 ROS generation, identical exposures were carried out in the presence of
 344 TPEN.

Zn^{2+} chelation has relatively little effect on fluorescence increases in
 345 2 mM $[\text{Ca}^{2+}]_e$ (supplemental Fig. S3). However, it may be difficult to re-
 346 solve contribution of Zn^{2+} to ROS generation under these conditions,
 347 since strong Ca^{2+} loading has been well documented to induce ROS
 348 production from extra-mitochondrial as well as mitochondrial sources.
 349 In contrast, when OGD was carried out in low $[\text{Ca}^{2+}]_e$, addition of TPEN
 350 significantly decreased the slope of the steep HET ΔF (to $m = 6.42 \pm$
 351 0.41 from 9.82 ± 0.82 in control; Fig. 3C).
 352

These observations indicate that Zn^{2+} makes a greater contribution
 353 to acute OGD induced ROS generation if the $[\text{Ca}^{2+}]_e$ is lowered, suggest-
 354 ing that Ca^{2+} has an inhibitory effect on this Zn^{2+} dependent ROS gen-
 355 eration. Ca^{2+} inhibition of Zn^{2+} dependent ROS generation could be
 356 most readily explained if there were competition between these ions
 357 for some site upstream from the Zn^{2+} triggered ROS release. One such
 358 site could be the MCU, with high levels of Ca^{2+} interfering with the pas-
 359 sage of Zn^{2+} through this channel.
 360

To test the role of the MCU in the OGD induced ROS generation, we
 361 first investigated the effects of RR on HET ΔF during OGD carried out in
 362 2 mM $[\text{Ca}^{2+}]_e$. RR application markedly slowed the ROS production
 363 (Fig. 3D). However, as RR accelerated Ca^{2+} deregulation and cell
 364

death in 2 mM $[Ca^{2+}]_e$, HET recording could not be carried out beyond 8–10 min. In addition, since high $[Ca^{2+}]_e$ was present during the OGD, it is not apparent whether the effects of RR are more due to block of Ca^{2+} and/or of Zn^{2+} entry through the MCU. For this reason, we next examined effects of RR on slices subjected to OGD in low $[Ca^{2+}]_e$. Addition of RR markedly slowed the steep phase of the HET ΔF , with effects that were qualitatively similar to but greater than those caused by TPEN (to $m = 1.96 \pm 0.33$ vs 4.1 ± 0.5 in control; Fig. 3E). The greater efficacy of RR than TPEN on the ROS production could reflect combined block of Ca^{2+} as well as of Zn^{2+} entry into mitochondria. This is likely consistent with our prior observations demonstrating synergistic effects of exogenous Ca^{2+} and Zn^{2+} loading on ROS production in cultured neurons (Sensi et al., 2000), and on swelling of isolated mitochondria (Jiang et al., 2001). If the effects of RR on ROS generation reflected only attenuation of Ca^{2+} entry and were independent of Zn^{2+} , we would expect to see additive attenuation of ROS generation when slices were treated with TPEN as well as RR. However, when experiments were performed with simultaneous TPEN and RR exposure, the decrease in the HET ΔF slope was no greater than with RR alone, providing strong evidence that the effect of RR is at least in part due to block of Zn^{2+} entry into the mitochondrial matrix through the MCU (Fig. 3F).

Discussion

Despite strong evidence for contributions of both Ca^{2+} and Zn^{2+} loading in ischemic neurodegeneration (Medvedeva et al., 2009; Randall and Thayer, 1992; Vander Jagt et al., 2008), our understanding of the respective contributions of these two cations has been limited, in part because of difficulties distinguishing these ions. Indeed, as the widely used fluorescent Ca^{2+} indicators are all also responsive to Zn^{2+} with greater molar potency than Ca^{2+} , it is likely that some effects previously attributed to Ca^{2+} are in fact Zn^{2+} mediated (Stork and Li, 2006). The advent of good Zn^{2+} selective fluorescent indicators combined with the use of Zn^{2+} chelators has enabled simultaneous detection of these cations and new investigations of their respective contributions (Devinney et al., 2005; Medvedeva et al., 2009). In recent studies of acute hippocampal slices subjected to OGD we documented the occurrence of early cytosolic Zn^{2+} rises that appeared to contribute to the onset of subsequent “ Ca^{2+} deregulation” events, which were causatively linked to a terminal loss of membrane integrity and cell death (Medvedeva et al., 2009).

It is apparent that mitochondria serve as important buffers for large cytosolic Ca^{2+} loads, reflecting uptake into the polarized mitochondrial matrix via the MCU (Wang and Thayer, 1996; Wang and Thayer, 2002), and numerous studies have reported Ca^{2+} overloading to induce mitochondrial dysfunction. However, as discussed in results, Zn^{2+} can also permeate the MCU, and appears to trigger effects including mitochondrial depolarization, ROS generation and swelling, apparently due to mitochondrial permeability transition pore (mPTP) induction, with far greater molar potency than Ca^{2+} (Gazaryan et al., 2007; Jiang et al., 2001; Sensi et al., 1999; Sensi et al., 2003; Wudarczyk et al., 1999). Suggesting that mitochondrial Zn^{2+} entry could contribute to injury, RR decreased both the ROS generation and neuronal injury caused by application of Zn^{2+} to cultured neurons (Clausen et al., 2013; Lozier et al., 2012).

Whereas above studies examined effects of exogenous Zn^{2+} , neuronal Zn^{2+} accumulation during ischemia likely reflects a combination of trans-synaptic passage of synaptically released Zn^{2+} , and Zn^{2+} release from cytosolic buffering proteins like metallothioneins (due to ischemia associated oxidative stress and acidosis) (Shuttleworth and Weiss, 2011), and emerging evidence suggests that this endogenous Zn^{2+} mobilization can also impact mitochondria. Indeed, endogenous Zn^{2+} accumulation appears to contribute to opening of channels in mitochondrial membranes and release of apoptotic mediators from mitochondria after in vivo ischemia (Bonanni et al., 2006; Calderone et al., 2004). We have found that oxidant induced mobilization of endogenous

Zn^{2+} can cause mitochondrial depolarization of cultured neurons (Sensi et al., 2003), and that early Zn^{2+} accumulation appears to contribute to irreversible mitochondrial depolarization in hippocampal slices subjected to OGD (Medvedeva et al., 2009).

The primary goal of present studies was to use MCU blockers to gain insights into the specific contribution of Zn^{2+} entry into mitochondria through these channels in acute ischemic neurodegeneration. Of note, prior studies using MCU blockers have yielded divergent effects, protecting isolated mitochondria from hypoxic injury (Schild et al., 2003), but having either beneficial effects, or deleterious effects associated with cytosolic Ca^{2+} overload in both neuronal and cardiac tissues depending upon the precise paradigm employed (Figueredo et al., 1991; Ruiz-Meana et al., 2006; Velasco and Tapia, 2000; Zhao et al., 2013). In line with these observations, we find that addition of RR during OGD carried out in physiological $[Ca^{2+}]_e$ in the absence of Ca^{2+} entry blockers accelerated the Ca^{2+} deregulation (Fig. 1B), likely by interfering with the ability of mitochondria to buffer large cytosolic Ca^{2+} loads, and possibly obscuring the ability to resolve beneficial effects of blocking mitochondrial Zn^{2+} entry. Supporting this interpretation, when Ca^{2+} entry was slowed, either by addition of Ca^{2+} entry blockers or by lowering the $[Ca^{2+}]_e$, MCU blockade accelerated the cytosolic Zn^{2+} rise (Figs. 2D,E), while significantly delaying the Ca^{2+} deregulation to a similar degree as Zn^{2+} chelation (Figs. 1C,D; 2A,B,C). Thus, while prior studies have indicated that endogenous Zn^{2+} can affect mitochondria, present observations that under conditions of attenuated Ca^{2+} entry, either Zn^{2+} chelation or MCU blockade is markedly protective provide new support for the hypothesis that passage of Zn^{2+} into mitochondria through the MCU is an early event in the neuronal injury cascade.

Interestingly, most studies of ischemic ROS generation have focused on the reperfusion phase, and although ROS production has been observed during OGD in both culture and slice models (Abramov et al., 2007; Frantseva et al., 2001), this has been relatively little studied. Using HET to image ROS generation in CA1 neurons during OGD reveals a distinct increase in fluorescence (ΔF) beginning shortly after OGD onset (Fig. 3A). Whereas multiple studies have reported that large intracellular Ca^{2+} loads can trigger mitochondrial ROS release (Bindokas et al., 1996; Carriedo et al., 1998; Dugan et al., 1995; Reynolds and Hastings, 1995), effects of Ca^{2+} on mitochondria are complex, and mechanisms of Ca^{2+} dependent enhancement of mitochondrial ROS release are poorly understood (Adam-Vizi and Starkov, 2010; Feissner et al., 2009; Peng and Jou, 2010). In the present studies, we were surprised to find that lowering Ca^{2+} , despite delaying the Ca^{2+} deregulation, actually accelerated the ROS generation (Fig. 3B). This observation provides evidence against the contention that Ca^{2+} loading is the only critical trigger of the ROS generation, and, taken together with observations that the ROS production was attenuated non-additively by either Zn^{2+} chelation or MCU blockade (Fig. 3C,E,F), lends new support for the idea that Zn^{2+} entry into mitochondria via the MCU is contributory.

Whereas it is clear that exogenous Zn^{2+} loading can trigger mitochondrial ROS generation (Sensi et al., 1999), present observations support the idea that endogenous Zn^{2+} does so as well. First, it is apparent that Zn^{2+} effects are not due simply to direct depolarization of mitochondria as a consequence of the charge carried by the Zn^{2+} entry, since absolute far greater levels of intracellular Ca^{2+} , which readily enters polarized mitochondria through the MCU, have less effect. Mechanisms of Zn^{2+} dependent mitochondrial ROS generation are uncertain, but like Ca^{2+} , there is evidence that it can induce block of the electron transport chain (Link and von Jagow, 1995; Skulachev et al., 1967), and can promote opening of the mPTP (Jiang et al., 2001; Wudarczyk et al., 1999), possibly after inducing potent (nM) and irreversible inhibition of key mitochondrial enzymes with critical roles in energy production and antioxidant defense (Gazaryan et al., 2007). In light of present observations that lowering $[Ca^{2+}]_e$ results in increased Zn^{2+} dependent ROS generation, might Zn^{2+} actually be the more significant of these

495 endogenous cations in the induction of mitochondrial ROS generation
496 during ischemia?

497 Conclusions/clinical implications

498 Stroke presents extreme therapeutic challenges, reflecting both dif-
499 ficulties in rapid delivery of therapeutic interventions to ischemic
500 brain and incomplete understanding of critical pathophysiological
501 events. Despite longstanding interest in contributions of Ca^{2+} , thera-
502 peutics targeting Ca^{2+} have yielded limited benefit, while further stud-
503 ies have highlighted important but poorly defined contributions of
504 Zn^{2+} . These Zn^{2+} dependent effects are likely of particular importance
505 in conditions like ischemia, wherein oxidative stress and acidosis impair
506 cytosolic Zn^{2+} buffering, such that modest cytosolic loading may result
507 in uptake into and disruption of mitochondrial function including ROS
508 generation (Clausen et al., 2013; Sensi et al., 2003). The emerging un-
509 derstanding of potent interactions of Zn^{2+} with mitochondria in early
510 phases of ischemia/OGD suggests mechanisms that may contribute to
511 early stages in the cell death cascade. Specifically, mitochondrial Zn^{2+}
512 uptake might hasten events including metabolic failure and ROS gener-
513 ation, resulting in the cell losing its ability to maintain Ca^{2+} ionic ho-
514 meostasis, with the result that Ca^{2+} deregulation occurs, triggering
515 catastrophic cell damage including loss of membrane integrity, likely
516 in large part via activation of catabolic enzymes. Furthermore, we sug-
517 gest that these events, if appropriately targeted, have the potential to
518 delay the onset of energy failure occurring upstream to the occurrence
519 of irreversible injury.

520 Although present results support an early role of mitochondrial
521 Zn^{2+} entry through the MCU in these events, since MCU blockade
522 may itself promote increased cytosolic Ca^{2+} and Zn^{2+} loading, MCU
523 blockers alone may not prove effective against acute ischemic injury.
524 Perhaps optimal interventions will use other approaches to either di-
525 minish Zn^{2+} accumulation within mitochondria, or protect mitochon-
526 dria from the deleterious effects of Zn^{2+} . Alternatively, MCU blockers
527 might prove to be effective when combined with other interventions
528 that either diminish the magnitude of the Ca^{2+} load (as suggested by
529 present observations using Ca^{2+} entry blockers), or antagonize the inju-
530 rious effects of cytosolic Ca^{2+} or Zn^{2+} loads (like inhibitors of Ca^{2+} de-
531 pendent catabolic enzymes or Zn^{2+} dependent signaling cascades)
532 (Shuttleworth and Weiss, 2011). It is hoped that with the right set of in-
533 terventions, early Zn^{2+} dependent mitochondrial dysfunction can be ab-
534 rogated, permitting greater opportunity for recovery from brain ischemia.

535 Supplementary data to this article can be found online at <http://dx.doi.org/10.1016/j.nbd.2014.04.011>.

537 Acknowledgments

538 Supported by NIH grants T32 NS45540 (Y.V.M.), R01 NS065219
Q11 (J.H.W.). We thank Jenny Truong for excellent help with animal care
540 and breeding.

541 References

- 542 Abramov, A.Y., Scorziello, A., Duchen, M.R., 2007. Three distinct mechanisms generate
543 oxygen free radicals in neurons and contribute to cell death during anoxia and reox-
544 ygenation. *J. Neurosci.* 27, 1129–1138.
- 545 Adam-Vizi, V., Starkov, A.A., 2010. Calcium and mitochondrial reactive oxygen species
546 generation: how to read the facts. *J. Alzheimers Dis.* 20 (Suppl. 2), S413–S426.
- 547 Bernardi, P., 1999. Mitochondrial transport of cations: channels, exchangers, and perme-
548 ability transition. *Physiol. Rev.* 79, 1127–1155.
- 549 Bindokas, V.P., et al., 1996. Superoxide production in rat hippocampal neurons: selective
550 imaging with hydroethidine. *J. Neurosci.* 16, 1324–1336.
- 551 Bonanni, L., et al., 2006. Zinc-dependent multi-conductance channel activity in mitochon-
552 dria isolated from ischemic brain. *J. Neurosci.* 26, 6851–6862.
- 553 Calderone, A., et al., 2004. Late calcium EDTA rescues hippocampal CA1 neurons from
554 global ischemia-induced death. *J. Neurosci.* 24, 9903–9913.
- 555 Carriedo, S.G., et al., 1998. Rapid Ca^{2+} entry through Ca^{2+} -permeable AMPA/kainate
556 channels triggers marked intracellular Ca^{2+} rises and consequent oxygen radical
557 production. *J. Neurosci.* 18, 7727–7738.

- Carter, R.E., et al., 2011. Spreading depression and related events are significant sources
of neuronal Zn^{2+} release and accumulation. *J. Cereb. Blood Flow Metab.* 31, 558–560.
- Chan, P.H., 2001. Reactive oxygen radicals in signaling and damage in the ischemic brain.
J. Cereb. Blood Flow Metab. 21, 2–14.
- Clausen, A., et al., 2013. Mechanisms of rapid reactive oxygen species generation in re-
sponse to cytosolic Ca^{2+} or Zn^{2+} loads in cortical neurons. *PLoS ONE* 8, e83347.
- Devinney 2nd, M.J., Reynolds, I.J., Dineley, K.E., 2005. Simultaneous detection of intracel-
lular free calcium and zinc using fura-2FF and FluoZin-3. *Cell Calcium* 37, 225–232.
- Dineley, K.E., Votyakova, T.V., Reynolds, I.J., 2003. Zinc inhibition of cellular energy pro-
duction: implications for mitochondria and neurodegeneration. *J. Neurochem.* 85, 567–569.
- Dugan, L.L., et al., 1995. Mitochondrial production of reactive oxygen species in cortical
neurons following exposure to N-methyl-D-aspartate. *J. Neurosci.* 15, 6377–6388.
- Feissner, R.F., et al., 2009. Crosstalk signaling between mitochondrial Ca^{2+} and ROS.
Front. Biosci. 14, 1197–1218.
- Figueredo, V.M., et al., 1991. Postischemic reperfusion injury in the isolated rat heart: ef-
fect of ruthenium red. *Cardiovasc. Res.* 25, 337–342.
- Frantseva, M.V., Carlen, P.L., Perez Velazquez, J.L., 2001. Dynamics of intracellular calcium
and free radical production during ischemia in pyramidal neurons. *Free Radic. Biol. Med.* 31, 1216–1227.
- Frederickson, C.J., Hernandez, M.D., McGinty, J.F., 1989. Translocation of zinc may contrib-
ute to seizure-induced death of neurons. *Brain Res.* 480, 317–321.
- Gazaryan, I.G., et al., 2007. Zinc irreversibly damages major enzymes of energy production
and antioxidant defense prior to mitochondrial permeability transition. *J. Biol. Chem.* 282, 24373–24380.
- Jiang, D., et al., 2001. Zn^{2+} induces permeability transition pore opening and release of
pro-apoptotic peptides from neuronal mitochondria. *J. Biol. Chem.* 276, 47524–47529.
- Kirichok, Y., Krapivinsky, G., Clapham, D.E., 2004. The mitochondrial calcium uniporter is a
highly selective ion channel. *Nature* 427, 360–364.
- Koh, J.Y., et al., 1996. The role of zinc in selective neuronal death after transient global ce-
rebral ischemia. *Science* 272, 1013–1016.
- Kuroda, S., Siesjo, B.K., 1997. Reperfusion damage following focal ischemia: pathophysiol-
ogy and therapeutic windows. *Clin. Neurosci.* 4, 199–212.
- Link, T.A., von Jagow, G., 1995. Zinc ions inhibit the QP center of bovine heart mitochon-
drial bcl complex by blocking a protonatable group. *J. Biol. Chem.* 270, 25001–25006.
- Lozier, E.R., et al., 2012. Stimulation of kainate toxicity by zinc in cultured cerebellar gran-
ule neurons and the role of mitochondria in this process. *Toxicol. Lett.* 208, 36–40.
- Malaiyandi, L.M., et al., 2005. Direct visualization of mitochondrial zinc accumulation re-
veals uniporter-dependent and -independent transport mechanisms. *J. Neurochem.* 93, 1242–1250.
- Matlib, M.A., et al., 1998. Oxygen-bridged dinuclear ruthenium amine complex specific-
ally inhibits Ca^{2+} uptake into mitochondria in vitro and in situ in single cardiac
myocytes. *J. Biol. Chem.* 273, 10223–10231.
- Medvedeva, Y.V., et al., 2009. Intracellular Zn^{2+} accumulation contributes to synaptic
failure, mitochondrial depolarization, and cell death in an acute slice oxygen–glucose
deprivation model of ischemia. *J. Neurosci.* 29, 1105–1114.
- Moore, C.L., 1971. Specific inhibition of mitochondrial Ca^{++} transport by ruthenium red.
Biochem. Biophys. Res. Commun. 42, 298–305.
- Peng, T.L., Jou, M.J., 2010. Oxidative stress caused by mitochondrial calcium overload. *Ann. N. Y. Acad. Sci.* 1201, 183–188.
- Randall, R.D., Thayer, S.A., 1992. Glutamate-induced calcium transient triggers delayed
calcium overload and neurotoxicity in rat hippocampal neurons. *J. Neurosci.* 12, 610–611.
- Reynolds, I.J., Hastings, T.G., 1995. Glutamate induces the production of reactive oxygen
species in cultured forebrain neurons following NMDA receptor activation. *J. Neurosci.* 15, 3318–3327.
- Rothman, S.M., Olney, J.W., 1986. Glutamate and the pathophysiology of hypoxic–is-
chemic brain damage. *Ann. Neurol.* 19, 105–111.
- Ruiz-Meana, M., et al., 2006. Mitochondrial Ca^{2+} uptake during simulated ischemia does
not affect permeability transition pore opening upon simulated reperfusion. *Cardiovasc. Res.* 71, 715–724.
- Saris, N.E., Niva, K., 1994. Is Zn^{2+} transported by the mitochondrial calcium uniporter?
FEBS Lett. 356, 195–198.
- Schild, L., et al., 2003. Brain mitochondria are primed by moderate Ca^{2+} rise upon
hypoxia/reoxygenation for functional breakdown and morphological disintegration.
J. Biol. Chem. 278, 25454–25460.
- Sensi, S.L., et al., 1999. Preferential Zn^{2+} influx through Ca^{2+} -permeable AMPA/kainate
channels triggers prolonged mitochondrial superoxide production. *Proc. Natl. Acad. Sci. U. S. A.* 96, 2414–2419.
- Sensi, S.L., Yin, H.Z., Weiss, J.H., 2000. AMPA/kainate receptor-triggered Zn^{2+} entry into
cortical neurons induces mitochondrial Zn^{2+} uptake and persistent mitochondrial
dysfunction. *Eur. J. Neurosci.* 12, 3813–3818.
- Sensi, S.L., et al., 2003. Modulation of mitochondrial function by endogenous Zn^{2+} pools.
Proc. Natl. Acad. Sci. U. S. A. 100, 6157–6162.
- Shuttleworth, C.W., Weiss, J.H., 2011. Zinc: new clues to diverse roles in brain ischemia.
Trends Pharmacol. Sci. 32, 480–486.
- Siesjo, B.K., 1988. Historical overview. Calcium, ischemia, and death of brain cells. *Ann. N. Y. Acad. Sci.* 522, 638–661.
- Skulachev, V.P., et al., 1967. Inhibition of the respiratory chain by zinc ions. *Biochem. Biophys. Res. Commun.* 26, 1–6.
- Stork, C.J., Li, Y.V., 2006. Intracellular zinc elevation measured with a “calcium-specific” in-
dicator during ischemia and reperfusion in rat hippocampus: a question on calcium
overload. *J. Neurosci.* 26, 10430–10437.
- Tapia, R., Velasco, I., 1997. Ruthenium red as a tool to study calcium channels, neuronal
death and the function of neural pathways. *Neurochem. Int.* 30, 137–147.

- 644 Tonder, N., et al., 1990. Possible role of zinc in the selective degeneration of dentate hilar
645 neurons after cerebral ischemia in the adult rat. *Neurosci. Lett.* 109, 247–252.
- 646 Vander Jagt, T.A., Connor, J.A., Shuttleworth, C.W., 2008. Localized loss of Ca²⁺ homeosta-
647 sis in neuronal dendrites is a downstream consequence of metabolic compromise
648 during extended NMDA exposures. *J. Neurosci.* 28, 5029–5039.
- 649 Velasco, I., Tapia, R., 2000. Alterations of intracellular calcium homeostasis and mitochon-
650 drial function are involved in ruthenium red neurotoxicity in primary cortical cul-
651 tures. *J. Neurosci. Res.* 60, 543–551.
- 652 Wang, G.J., Thayer, S.A., 1996. Sequestration of glutamate-induced Ca²⁺ loads by mito-
chondria in cultured rat hippocampal neurons. *J. Neurophysiol.* 76, 1611–1621.
- Wang, G.J., Thayer, S.A., 2002. NMDA-induced calcium loads recycle across the mitochon-
drial inner membrane of hippocampal neurons in culture. *J. Neurophysiol.* 87, 740–749.
- Wei, G., et al., 2004. Characterization of extracellular accumulation of Zn²⁺ during ische-
mia and reperfusion of hippocampus slices in rat. *Neuroscience* 125, 867–877.
- Weiss, J.H., Sensi, S.L., Koh, J.Y., 2000. Zn(2+): a novel ionic mediator of neural injury in
brain disease. *Trends Pharmacol. Sci.* 21, 395–401.
- Wudarczyk, J., Debska, G., Lenartowicz, E., 1999. Zinc as an inducer of the membrane
permeability transition in rat liver mitochondria. *Arch. Biochem. Biophys.* 363,
1–8.
- Yamamoto, S., et al., 1997. Factors that reverse the persistent depolarization produced by
deprivation of oxygen and glucose in rat hippocampal CA1 neurons in vitro. *J.*
Neurophysiol. 78, 903–911.
- Yin, H.Z., et al., 2002. Blockade of Ca²⁺-permeable AMPA/kainate channels decreases ox-
ygen–glucose deprivation-induced Zn²⁺ accumulation and neuronal loss in hippo-
campal pyramidal neurons. *J. Neurosci.* 22, 1273–1279.
- Zhao, Q., et al., 2013. The role of the mitochondrial calcium uniporter in cerebral ische-
mia/reperfusion injury in rats involves regulation of mitochondrial energy metabo-
lism. *Mol. Med. Rep.* 7, 1073–1080.

UNCORRECTED PROOF